ResearchGate

See discussions, stats, and author profiles for this publication at: https://www.researchgate.net/publication/256200302

Fine Modulation of the Respiratory Syncytial Virus M2-1 Protein Quaternary Structure by Reversible Zinc Removal from Its Cys(3)-His(1) Motif

ARTICLE *in* BIOCHEMISTRY · AUGUST 2013

Impact Factor: 3.02 · DOI: 10.1021/bi401029q · Source: PubMed

CITATIONS
2

READS
48

6 AUTHORS, INCLUDING:

Sebastián Andrés Esperante
Fundación Instituto Leloir
16 PUBLICATIONS **209** CITATIONS
SEE PROFILE

Guilherme A. P. de Oliveira
Federal University of Rio de Janeiro
24 PUBLICATIONS **119** CITATIONS
SEE PROFILE

Jerson L Silva
Federal University of Rio de Janeiro
182 PUBLICATIONS **5,145** CITATIONS
SEE PROFILE

Gonzalo de Prat-Gay
Fundación Instituto Leloir
96 PUBLICATIONS **1,822** CITATIONS
SEE PROFILE

Available from: Guilherme A. P. de Oliveira
Retrieved on: 31 January 2016

BIOCHEMISTRY
including biophysical chemistry & molecular biology

Article

pubs.acs.org/biochemistry

Fine Modulation of the Respiratory Syncytial Virus M_{2-1} Protein Quaternary Structure by Reversible Zinc Removal from Its Cys_3-His_1 Motif

Sebastián A. Esperante,[†] María G. Noval,[†] Tamara A. Altieri,[†] Guilherme A. P. de Oliveira,[‡] Jerson L. Silva,[‡] and Gonzalo de Prat-Gay*,[†]

[†]Protein Structure−Function and Engineering Laboratory, Fundación Instituto Leloir and IIBA-Conicet, Patricias Argentinas 435, (1405) Buenos Aires, Argentina

[‡]Programa de Biologia Estrutural, Instituto de Bioquímica Médica, Instituto Nacional de Biologia Estrutural e Bioimagem, Centro Nacional de Ressonância Magnética Nuclear Jiri Jonas, Universidade Federal do Rio de Janeiro, 21941-902, Rio de Janeiro, Brazil

ABSTRACT: Human respiratory syncytial virus (hRSV) is a worldwide distributed pathogen that causes respiratory disease mostly in infants and the elderly. The M_{2-1} protein of hRSV functions as a transcription antiterminator and partakes in virus particle budding. It is present only in *Pneumovirinae*, namely, *Pneumovirus* (RSV) and *Metapneumovirus*, making it an interesting target for specific antivirals. hRSV M_{2-1} is a tight tetramer bearing a Cys_3-His_1 zinc-binding motif, present in Ebola VP30 protein and some eukaryotic proteins, whose integrity was shown to be essential for protein function but without a biochemical mechanistic basis. We showed that removal of the zinc atom causes dissociation to a monomeric apo-M_{2-1} species. Surprisingly, the secondary structure and stability of the apo-monomer is indistinguishable from that of the M_{2-1} tetramer. Dissociation reported by a highly sensitive tryptophan residue is much increased at pH 5.0 compared to pH 7.0, suggesting a histidine protonation cooperating in zinc removal. The monomeric apo form binds RNA at least as well as the tetramer, and this interaction is outcompeted by the phosphoprotein P, the RNA polymerase cofactor. The role of zinc goes beyond stabilization of local structure, finely tuning dissociation to a fully folded and binding competent monomer. Removal of zinc is equivalent to the disruption of the motif by mutation, only that the former is potentially reversible in the cellular context. Thus, this process could be triggered by a natural chelator such as glutathione or thioneins, where reversibility strongly suggests a modulatory role in the participation of M_{2-1} in the assembly of the polymerase complex or in virion budding.

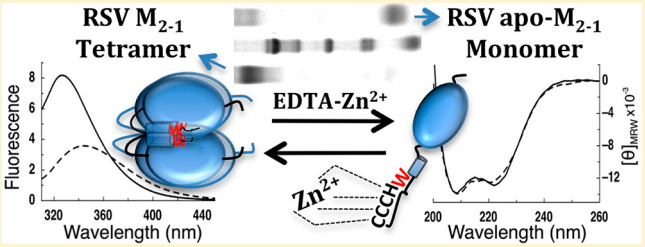

Human respiratory syncytial virus (hRSV) is a major cause of pediatric viral respiratory tract infections, with a peak age ranging from 3 to 6 months, and is the leading cause of infant hospitalization in industrialized countries.[1] Recently, RSV has also been associated with severe morbidity in the elderly, immunocompromised, and adults with underlying chronic cardiopulmonary disease.[2] A monoclonal antibody palivizumab is indicated for RSV prevention in high-risk infants, including premature babies and infants with chronic lung disease and congenital heart disease.[3] For healthy newborns with no underlying risk factors, no immunoprophylaxis or active vaccination is currently available. Ribavirin has been used to treat severe RSV disease, despite its effectiveness is questionable.[4]

The RSV virus belongs to the order *Mononegavirales*, family *Paramyxoviridae*, genus *Pneumovirus*.[5] The RSV genome consists of an ∼15 kb single-stranded nonsegmented negative-sense RNA which is encapsidated by the nucleocapsid (N) protein. The resulting ribonucleoprotein complex (N-RNA) is the template for transcription and replication of the viral genome by the RNA-dependent RNA polymerase complex which comprises the large polymerase protein L, the phosphoprotein P, and the antiterminator factor M_{2-1}.[5]

The RSV M_{2-1} protein acts as a transcription elongation factor increasing the processivity of the viral RNA polymerase, preventing premature termination during transcription[6] and also enhancing the ability of the polymerase to read through transcription termination signals, thereby acting as a transcription antiterminator.[7] This antiterminator activity varies at the different gene junctions[8] and might be important in determining the amount of polymerase delivered to promoter-distal genes.[7,8] In addition to its role in transcription, the M_{2-1} protein interacts with the matrix protein M, allowing its incorporation into cytoplasmic inclusion bodies.[9] Thus, recruitment of the M protein through its interaction with M_{2-1} might mediate viral assembly and budding.[10]

It has been shown that the M_{2-1} protein forms a tight tetramer in solution with an apparent dissociation constant

Received: July 30, 2013
Revised: August 26, 2013
Published: August 28, 2013

ACS Publications © 2013 American Chemical Society

dx.doi.org/10.1021/bi401029q | *Biochemistry* 2013, 52, 6779−6789

(K_D) of 10^{-28} M^3 at pH 7.0 and the tetramer affinity is strongly governed by pH.[11,12] As a result, lowering the pH destabilizes the tetramer, inducing its dissociation. The M_{2-1} protein contains a CCCH motif ($CX_7CX_5CX_3H$) near the amino terminus, spanning from residues 7 to 25, which has been shown to coordinate zinc.[12] Mutations of three residues of the CCCH motif (Cys7, Cys15, and His25) prevented the M_{2-1} protein from enhancing transcriptional read-through and interacting with the nucleocapsid protein, demonstrating that the CCCH motif is essential to maintain the functional integrity of the M_{2-1} protein.[13] Moreover, the three cysteines of the CCCH motif are essential for viral viability as inferred from mutational studies,[14] and some positive charged residues within the motif (Leu16 and Asn17) had been shown to be essential for M_{2-1} protein function.[15]

The RSV M_{2-1} is an RNA binding protein that binds to long RNAs with no sequence specificity but specifically interacts with short RNAs with an apparent K_D in the nM range.[16] Using a series of GST-M_{2-1} deletion mutants, the M_{2-1}/M_{2-1} interaction was studied by the ability of a histidine-tagged M_{2-1} protein (His-M_{2-1}) to copurify with GST-M_{2-1}. The homo-oligomerization domain was mapped between residues 35 to 58, and its deletion resulted in the loss of transcription antiterminator activity, suggesting that this activity depends on the tetrameric nature of M_{2-1}.[11] An N-terminal deletion mutant of 31 residues comprising the CCCH motif retained the ability to oligomerize.

Using a similar approach, Tran et al.[11] mapped the RNA- and P-binding domains of M_{2-1}, both situated between residues 59 and 153. Interestingly, an N-terminal deletion mutant of 58 residues (M_{2-1} Δ58N), which lacks the CCCH motif and the oligomerization domain, retains its ability to bind RNA and P. This indicates that the monomeric form of M_{2-1} was able to interact with P and RNA despite its loss of antiterminator activity in functional assays. The monomeric M_{2-1} Δ58N showed a far-UV CD spectrum similar to that of full-length M_{2-1}, typical of α-helical proteins, indicating that the secondary structure was not adversely affected by the deletion.

The solution structure of a monomeric fragment of human RSV M_{2-1}, spanning residues 58 to 177 (M_{2-1} 58−177), was determined by NMR. The M_{2-1} 58−177 fragment contains a single globular domain comprising six α-helices, which is structurally homologous to the α-helix bundle fold of EBOV VP30CTD.[17] The N-terminus (Ser58-Lys74) of M_{2-1} 58−177, which links to the upstream oligomerization domain, is disordered. The M_{2-1} 58−177 fragment was able to bind to different RSV short (negative or positive sense) RNAs with an apparent dissociation constant ranging from 2.5 μM to 600 μM, while short positive sense A-rich RSV RNAs sequences were recognized with higher affinity. The monomeric M_{2-1} 58−177 binds P and RNA by two distinct binding surfaces that partially overlap, located on a positively charged face.[18] By isothermal titration calorimetry (ITC) experiments, the dissociation constant of the interaction of M_{2-1} 58−177 and P was shown to be 3 μM.[18] However, the K_D estimated by fluorescence anisotropy titrations of the full length M_{2-1} and P was ∼10 nM with a 1:1 stoichiometry. The difference in affinity could be due to a binding cooperative effect of full length tetrameric M_{2-1}.[19]

Distinct cysteine zinc fingers have been classified and grouped according to the arrangement and number of the conserved cysteine and/or histidine residues involved in zinc coordination (CCHH; CCCC; CCHC; and CCCH families.).[20,21] In many cases, these zinc-binding motifs mediate protein−protein and protein nucleic acid interactions. One example of both activities has been shown for the Ikaros transcription factor, which contains two clusters of CCHH zinc finger motifs: an N terminal cluster of 3 to 4 zinc fingers that bind DNA and a C terminal cluster of 2 zinc fingers that mediate homodimerization and heterotypic interactions. The Ikaros protein requires zinc ions to maintain intersubunit interaction.[22]

CCCH type zinc fingers were recently identified in a number of RNA binding proteins, from viral to eukaryotic proteins.[21] They are heterogeneous regarding the number of CCCH motifs contained. The Nup475/TTP/TIS11 protein contains two tandemly repeated CCCH zinc-binding domains ($CX_8CX_5CX_3H$) that bind to AU-rich elements in the 3′-untranslated regions of certain mRNAs and destabilizes them, promoting their deadenylation and degradation.[23] A single CCCH domain is capable of binding single-stranded RNA with considerable affinity and selectivity.[24] The NMR structure of a single CCCH domain from Nup475 reveals the presence of a short α-helix between the first and second cysteines that are coordinated to zinc, but little or no other secondary structure is present.[25] Another mammalian protein belonging to the TIS11 family, named TIS11d, harbors two CCCH motifs, which fold independently to form small, compact domains connected by a linker sequence. The polypeptide backbone adopts little regular secondary structure, and there is a short α-helix immediately after the first cysteine ligand and a turn of 3_{10}-helix between the second and third cysteine ligands.[26] Each zinc motif binds to the RNA sequence 5′ UAUU 3′ through a combination of electrostatic and hydrogen-bonding interactions, with intercalative stacking between conserved aromatic side chains and the RNA bases.[26] The crystal structure of the CCCH motif of the mRNA splicing component Cwc2 revealed a fold very similar to that of Tis11d with few secondary structure elements.[27]

The Ebola virus (a Filovirus in the *Mononegaviridae* order) transcription activator VP30 shows some structural and functional similarities with the RSV M_{2-1} protein. VP30 is an RNA binding protein[28] that contains a CCCH zinc-binding motif comprising residues 68 to 95. Substitutions of the coordinating residues led to the loss of zinc-binding capacity and loss of function.[29] A region spanning from residues 94 to 112 was shown to be essential for oligomerization, and some mutations within this region resulted in oligomeric-deficient and loss-of-function VP30 protein.[30] Later, it was found that VP30 homo-oligomerization leads to hexamers *in vitro* and *in vivo*.[17] Peptide and small-molecule inhibitors that might interfere with VP30 homo-oligomerization in order to prevent VP30 activity have been proposed as potential targets for antiviral treatment.[17,30]

The CCCH zinc-binding motif is found in the M_{2-1} proteins of all Pneumoviruses and is essential to maintain the functional integrity of M_{2-1} and for viral viability[13,14] However, the exact role that the CCCH motif plays in M_{2-1} protein structure and function is still unknown.

In the present work, we investigated the effect of zinc in the overall structure and binding properties of the M_{2-1} antiterminator. Removal of the zinc atom by EDTA leads rapidly to dissociation into monomeric species, retaining the secondary and tertiary structures, showing that the oligomerization is determined by the CCCH motif. The sensitivity of the reversible metal removal strongly suggests this biochemical

reaction as an important regulatory event in RSV gene function in infected cells. There is a combined effect of metal removal with pH, and glutathione shows the capacity to act as chelator for zinc. We discuss the results in connection with RSV function but find divergent examples of zinc-binding motifs converging in the modulation of protein association−dissociation.

EXPERIMENTAL PROCEDURES

Expression and Purification of the HRSV M_{2-1} Protein. The human RSV strain A M_{2-1} protein was recombinantly expressed and purified as previously described.[12] Briefly, C41(DE3) cells harboring the plasmid pRSETA M_{2-1} were grown in LB, and the protein expression was induced with 0.3 mM IPTG. The soluble protein was precipitated with 40% ammonium sulfate, resuspended, and purified with a combination of heparin ceramic hyperD column and preparative gel filtration (S200) chromatographies.

The M_{2-1} protein stock solution used was prepared as follows. Highly purified M_{2-1} was treated for 2 h at 25 °C with 10 mM DTT and dialyzed for 6 h against 50 mM sodium phosphate at pH 7.0, 0.3 M NaCl, 20 μM Zn_2SO_4, and 1 mM DTT. Then, it was dialyzed for 16 h with the same buffer without Zn_2SO_4. Protein concentration was determined spectrophotometrically using a molar extinction coefficient $\varepsilon_{280\ nm}$ = 13200 M^{-1} cm^{-1}. A ratio of 260:280 nm of ∼0.55 was indicative of minimum nucleic acid contamination. The protein concentration is expressed as monomer concentration. For the determination of metal content, M_{2-1} was separated from exogenous metals and DTT by gel filtration using a PD-10 column (Amersham Biosciencies).

Preparation of Reduced, Zinc-Free M_{2-1} (Apo-M_{2-1}). The apo-M_{2-1} protein used in the Zn uptake titration experiments (Figures 3 and 4) was prepared as follows: The purified M_{2-1} at 60 μM was incubated at room temperature for 16 h with 10 mM EDTA in 20 mM phosphate buffer at pH 7.0 containing 1.0 M Gdm·Cl and 10 mM DTT. Then, the preparation was loaded onto a PD10 column equilibrated in 20 mM sodium phosphate at pH 7.0 and 0.3 M NaCl. The apo-M_{2-1} protein was quantified by UV spectrophotometry at 280 nm, and the absence of zinc was determined by the PAR/PMPS assay (see below). For the Gdm·Cl induced unfolding experiments (Figures 5 and 6), apo-M_{2-1} was prepared in each incubation tube by adding 1 mM EDTA to 5 μM M_{2-1}. In EMSA experiments, 5 mM of EDTA was added to the binding reaction to M_{2-1} ranging from 1 to 16 μM (Figure 8). All chemical reagents used were of analytical grade (purchased from Sigma Aldrich or ICN), and all solutions were prepared using milli-Q water.

Determination of Zinc Concentrations Bound to M_{2-1}. Zinc concentrations were determined by spectrophotometric measurement of the metallochromic indicator 4-(2-pyridylazo)-resorcinol (PAR).[31] PAR binds zinc to form a $Zn(PAR)_2$ complex, which absorbs strongly at 500 nm ($\varepsilon_{500\ nm}$ = 66000 M^{-1} cm^{-1} in Hepes, pH 7.0). Purified 2 to 10 μM M_{2-1} or APO-M_{2-1}, without DTT, was first added to a solution containing 100 μM PAR reagent to measure weakly bound metal. To determine the amount of zinc bound to the protein, *p*-hydroxymercuriphenylsulfonic acid (PMPS) was added to release zinc from the metal center and allow the formation of the $Zn(PAR)_2$ complex. All chemical reagents used were of analytical grade (purchased from Sigma Aldrich or ICN), and all solutions were prepared using milli-Q water.

Size-Exclusion Chromatography. Size-exclusion chromatography was carried out on a Superdex 200 HR 10/30 (24 mL) column (GE Healthcare). The S200 column was calibrated with the following standard globular proteins: ferritin (440 kDa), catalase (232 kDa), BSA (67 kDa), ovalbumin (43 kDa), and chymotrypsinogen A (25 kDa) from a gel calibration kit (Pharmacia Biotech, Uppsala, Sweden). The void volume (Vo) and total volume (Vt) were determined by loading Blue Dextran and acetone, respectively. The buffers used in the runs are indicated in each case.

Dynamic Light Scattering. The determination of the hydrodynamic size distribution of M_{2-1} and apo-M_{2-1} by dynamic light scattering (DLS) was performed on a Zeta Sizer Nano S DLS device from Malvern Instruments (Malvern). The solutions were centrifuged at 14000*g* for 10 min at 4 °C and filtered with Ultrafree-MC microcentrifuge filters (0.22 μm, Millipore) before measurements were taken.

Circular Dichroism (CD) and Fluorescence Spectroscopy. Far-UV CD measurements were conducted on a Jasco J-810 spectropolarimeter using a Peltier temperature-controlled cell. Spectra were recorded between 200 and 260 nm at standard sensitivity, at a rate of 200 nm/min, a response time of 2 s, at a data pitch of 0.2 nm, and a bandwidth of 2 nm. All spectra were an average of at least 4 scans. Spectra of M_{2-1} at 5 μM were taken on a 0.1 cm path length cell. The ellipticity at 260 nm was subtracted from the other ellipticities as a baseline value. Raw data were converted to molar ellipticity using the following equation:

$$[\theta]\mathrm{MRW} = \frac{\mathrm{deg}}{[c] \times \#bonds \times L \times 10} \quad (1)$$

Where deg is the raw signal in millidegs, $[c]$ is protein concentration in molar units, #bonds is the number of peptide bonds (number of amino acids − 1), and L is the path length in cm.

Tryptophan fluorescence emission spectra were recorded on a Jasco FP-6500 spectrofluorometer with an excitation wavelength of 295 nm, and the emission spectrum was recorded from 310 to 450 nm. Fluorescence emission data were analyzed by first subtracting the buffer background at the appropriate Gdm·Cl concentration, and the center of spectral mass of the emission spectrum was quantified as follows:

$$\mathrm{CSM}\ (\mathrm{cm}^{-1}) = \frac{\sum (\upsilon_i \times F_i)}{\sum F_i} \quad (2)$$

where F_i is the fluorescence emission at wavenumber υ_i, and the summation is carried out over the range of measured values of F. Spectra of M_{2-1} at 5 μM were taken in a 4 mm path length quartz with excitation/emission slits set at 5 nm/10 nm. All of the spectroscopic measurements were performed at 20 °C.

Glutaraldehyde Cross-Linking. M_{2-1} at 2 to 5 μM was incubated for 16 h at room temperature at a given Gdm·Cl concentration (with or without EDTA 1 mM). The samples were then treated with 0.1% glutaraldehyde and incubated for 30 s at room temperature. The reactions were stopped by adding 100 mM Tris·HCl at pH 7.0 and 50 mM $NaBH_4$. The samples were diluted 10 times with 20 mM sodium phosphate at pH 7.0 and 0.3 M NaCl and precipitated on ice with 10% TCA (trichloroacetic acid) for 30 min. The samples were then centrifuged at 14000*g* for 10 min at 4 °C, and the pellet was washed twice with ice-cold acetone and resuspended in 20 μL of SDS sample buffer. Finally, the samples were boiled and

dx.doi.org/10.1021/bi401029q | *Biochemistry* 2013, 52, 6779−6789

loaded onto a 12.5% SDS−polyacrylamide gel and stained with Coomasie-blue.

Guanidinium Chloride (Gdm·Cl) Induced Denaturation Experiments. Experiments at pH 7.0 were performed by equilibrating the M_{2-1} protein in tubes containing 20 mM sodium phosphate at pH 7.0, 0.2 M NaCl, 1 mM DTT, and increasing concentrations of Gdm·Cl. Experiments at pH 5.0 were performed in 20 mM sodium acetate at pH 5.0, 0.2 M NaCl, 1 mM DTT, and increasing concentrations of Gdm·Cl. The Gdm·Cl stock solutions contained 7.5 M Gdm·Cl, either in 20 mM sodium phosphate at pH 7.0 or 20 mM sodium acetate at pH 5.0. In the case of apo-M_{2-1}unfolding reactions, 1 mM EDTA was added to each sample to chelate zinc. The samples were incubated for 16 h at 20 °C prior to measurement. The final M_{2-1} concentration was 5 μM in both cases.

Data Analysis and Fitting of Apo-M_{2-1} Equilibrium Unfolding. Considering that we had physical evidence by DLS, SEC, and glutaraldehyde cross-linking (Figures 2 3, 5, and 6) that the EDTA-treated M_{2-1} oligomeric state was monomeric, we assumed a simple two-state unfolding model in order to estimate the thermodynamic parameters for the transition:[32]

$$N \overset{K_U}{\leftrightarrow} U$$

Gdm·Cl denaturation curves were fit to a two-state model considering native (N) and unfolded (U) monomers. The molar ellipticity at 222 nm signal was fit to the following equation:

$$y = (N_{in} + N_m \times [\text{Gdm·Cl}]) \times f_N + (U_{in} + U_m \times [\text{Gdm·Cl}]) \times f_U \quad (3)$$

where y is the measured signal, N_{in} and U_{in} are the spectroscopic signal of the native and unfolded states, and N_m and U_m account for the lineal variations of the signal with [Gdm·Cl]. The fractions of the native and unfolded species (f_N and f_U) are defined as follows:

$$f_N = \frac{1}{1 + K_U}; \quad f_U = \frac{K_U}{1 + K_U}; \quad K_U = e^{-(\Delta G^{H20} - m\cdot[\text{GdmCl}])/RT} \quad (4)$$

where R is the gas constant, and T the temperature, K_U and ΔG^{H20} are the equilibrium unfolding constant and free energy of unfolding, respectively, and m is the m-value for the transition. Parameters were estimated from fitting the CD data.

GSH/GSSG Redox Potential and pH Dependence. Measurements were performed in 20 mM sodium phosphate at pH 7.0 or 20 mM sodium acetate at pH 5.0, both with 0.2 M NaCl and a 5 mM final concentration of [GSH]/[GSSG] mixtures. Six micromolar M_{2-1} protein without DTT was incubated for 16 h at 20 °C in each condition, which consists of nine different [GSH]/[GSSG] ratios ranging from 1 to 300. To test the pH dependence over different GSH/GSSG redox conditions, the measurements were performed in a broad range buffer containing 50 mM Tris·Cl, 25 mM MES, and 25 mM sodium acetate with 0.2 M NaCl and a 5 mM final concentration of [GSH]/[GSSG] mixtures. Samples of M_{2-1} at 6 μM were incubated in the corresponding buffer without glutathione and with [GSH]/[GSSG] ratios of 1, 100, and 300. The pH values tested ranges from 4.4 to 8.4.

Electrophoretic Mobility-Shift Assay (EMSA). One milligram of sodium-tRNA (baker yeast tRNA, Sigma) was dissolved in 1 mL of milli-Q H_20. After the addition of 5 mM EDTA, the tRNA sample was incubated at 80 °C for 20 min and cooled at room temperature. Then, the tRNA sample was stepwise dialyzed against 4 L of 10 mM sodium phosphate at pH 7.0 at 4 °C. The concentration of tRNA was determined based on the assumption that a 40 μg/mL solution has an absorbance of 1.0 at 260 nm. An average molecular weight of 25000 g/mol was considered for the tRNA molecules to calculate the molar concentration. Thus, 40 μg/mL = 1.6 μM = 1 $D.O_{260\ nm}$.

tRNA (1.5 μM) was incubated with increasing concentrations of purified M_{2-1} protein (indicated in Figure 8) in binding buffer that contained 20 mM HEPES at pH 7.0, 5% glycerol, 0.1 M NaCl, and 10 μM M $ZnCl_2$. To prepare the tRNA/apo-M_{2-1} binding reactions, 5 mM EDTA was added to each incubation tube, and no zinc was included. For competition experiments, increasing amounts of highly purified RSV P protein were added to the binding buffer containing 1.5 μM tRNA and 10 μM M_{2-1}. To prepare apo-M_{2-1}, 5 mM EDTA was added to each incubation tube. All of the samples were incubated at 4 °C for 2, 6, and 16 h, loaded on a 1.5% agarose gel, and electrophoresed in TA (40 mM Tris and 20 mM acetic acid) buffer at pH 8.0 at 60 V for 1 h at room temperature. The tRNA was visualized with ethidium bromide staining and a gel UV lamp. The concentration of the M_{2-1} protein was expressed as monomer concentration. The human RSV P protein was recombinantly expressed in bacteria, purified, and quantified as previously described.[19]

RESULTS

Zinc Removal from the M_{2-1} Tetramer Leads to a Stable Apo-Monomer. Since our first goal was to evaluate the role of the zinc on structure, stability, and ligand binding of the M_{2-1} tetramer, we aimed at removing the metal by treatment with a high affinity chelator such as EDTA (K_a = 10 ^{16} M). Treatment of M_{2-1} with EDTA caused a change in fluorescence spectra, shifting the maximum wavelength from 325 to 350 nm, indicative of the exposure of its unique tryptophan residue to the solvent, and in principle, the loss of tertiary structure through global unfolding (Figure 1A).

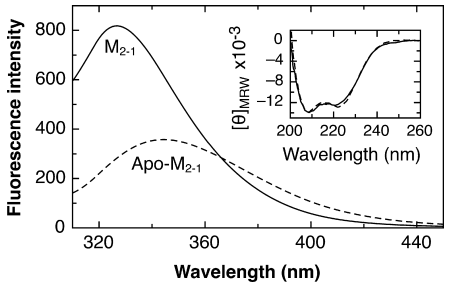

Figure 1. Zinc removal from the M_{2-1} tetramer changes the tryptophan environment without changing the secondary structure content. Tryptophan fluorescence emission spectra of M_{2-1} and apo-M_{2-1}. The M_{2-1} protein (2 μM) was incubated prior to measurements for 20 h at room temperature in 20 mM sodium phosphate (pH 7.0), 0.3 M NaCl, 1 mM DTT, either with 1 mM EDTA (Apo-M_{2-1}: dashed line) or without EDTA (M_{2-1}: solid line). Inset: Far-UV CD spectra of M_{2-1} (solid line) and apo-M_{2-1} (dashed line) prepared as described above.

dx.doi.org/10.1021/bi401029q | Biochemistry 2013, 52, 6779−6789

However, there was no change whatsoever in the secondary structure content as judged by far-UV CD (Figure 1A, inset), which indicates that the overall secondary structure is maintained and that the exposure of the tryptophan residue is not caused by global unfolding.

Kinetic analysis by fluorescence showed that both the intensity and tryptophan fluorescence center of spectral mass (CSM) changed concomitantly with an apparent half-life of ~10 h and the process is largely accelerated at 1.0 M of Gdm·Cl, with a half-life of ~30 min (Figure 2A). Analysis of the same experiment by chemical cross-linking with glutaraldehyde followed by SDS−PAGE confirmed the spectroscopic data and strongly suggested that dissociation from tetramer to monomer took place as a result of the zinc removal, accelerated by the addition of 1.0 M Gdm·Cl (Figure 2B). Size-exclusion chromatography experiments (Figure 2C) confirmed the dissociation of the M_{2-1} tetramer to the apo-monomer, which retains its full secondary structure content. According to the calibration of the column with globular proteins, the M_{2-1} tetramer (88 kDA) eluted as a globular protein of 110 kDa, while the apo-M_{2-1} monomer (22 kDa) eluted as a 28 kDa species. Finally, the dissociation was supported by dynamic light scattering (DLS) analysis of M_{2-1} and apo-M_{2-1} at 1.0 M Gdm·Cl (Figure 2C, inset). Both M_{2-1} and apo-M_{2-1} presented a homogeneous particle size distribution with a hydrodynamic diameter of 9.6 ± 1.9 nm and 5.8 ± 1.9 nm, corresponding to spherical proteins of 170 and 53 kDa, respectively.[33] Thus, both the tetrameric and monomeric M_{2-1} species were extended under the experimental conditions.

Once we demonstrated that zinc removal leads to M_{2-1} dissociation, we prepared the reduced zinc-depleted apo-M_{2-1} monomer in order to study metal reuptake and the reversibility of the tetramerization process. The apo-M_{2-1} was treated with an excess of zinc, and both fluorescence intensity and the tryptophan center of spectral mass were monitored over time (Figure 3A). There was a remarkably fast zinc reuptake, which was completed within the dead time for manual mixing, and this was slowed down in the presence of 1.0 M Gdm·Cl (Figure 3A), which was validated by the corresponding cross-linking-SDS−PAGE experiment at different time points after the addition of zinc to the apo-M_{2-1} monomer (Figure 3B). These results provide substantial evidence that the apo-monomer readily reuptakes zinc and returns to the native M_{2-1} tetramer, indicating that zinc uptake triggers M_{2-1} tetramer assembly.

Next, we carried out a titration experiment in which apo-M_{2-1} was titrated with increasing amounts of zinc and monitored by fluorescence spectroscopy (Figure 4). Apo-M_{2-1} displayed an increase in tryptophan fluorescence at 325 nm upon zinc binding that reached a maximum value at a zinc/apo-M_{2-1} ratio of ~1:1 (Figure 4A, inset). At this saturation point, the fluorescence spectra returned to that of the original M_{2-1} tetramer (Figure 4A).

When the titration was monitored by the changes in the tryptophan fluorescence CSM, the stoichiometry was slightly lower (0.75:1) (Figure 4B). This result may have several explanations: (i) that part of the population does not take up zinc and averages the titration, something not unexpected since the metal removal may not be fully completed, (ii) that the proximity of the now released cysteine side chains may oxidize, and (iii) that the tetramer assembly, reported by the tryptophan hydrophobic environment, could be completed before reaching a 1:1 (zinc:monomer) stoichiometry or (iv) that a combination of any of these processes occurs. As a complementary approach

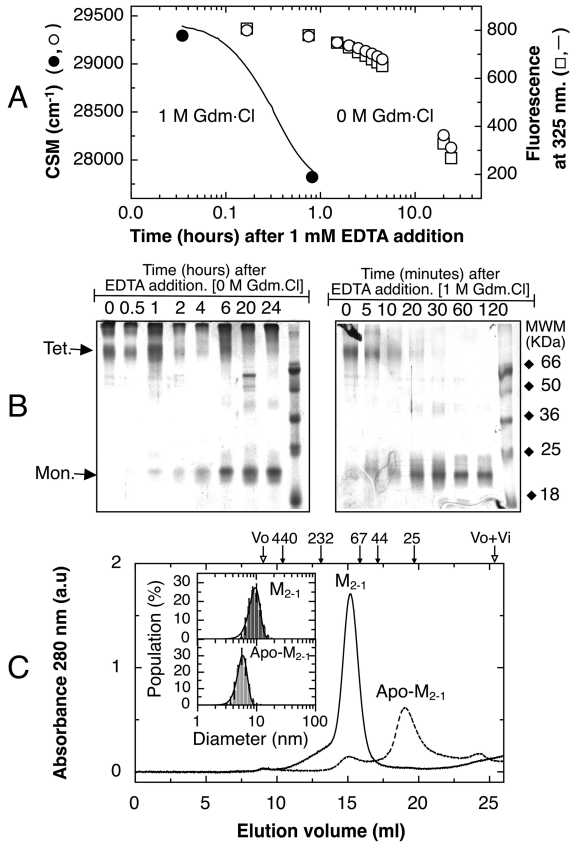

Figure 2. EDTA induced zinc release promotes M_{2-1} tetramer dissociation to monomer. (A) Changes in the tryptophan fluorescence center of spectral mass (CSM) (left Y axis) and in the fluorescence intensity at 325 nm (right Y axis) were monitored over time upon the addition of 1 mM EDTA to M_{2-1} (2 μM) in 20 mM sodium phosphate (pH 7.0), 0.3 M NaCl, 1 mM DTT containing either 0 M Gdm·Cl (○, CSM; □, fluorescence intensity at 325 nm) or 1.0 M Gdm·Cl (●, CSM; —, fluorescence intensity at 325 nm). The measurements were performed at 20 °C. (B) The samples in the same conditions described in 2A were subjected at different time points (indicated above the graph) to glutaraldehyde cross-linking and SDS−PAGE. The samples loaded in the left gel contained 0 M Gdm·Cl and in the right gel were incubated with 1.0 M Gdm·Cl. The molecular weights of the marker and the bands corresponding to tetramer and monomer are indicated. (C) Size exclusion chromatographies of M_{2-1} (solid line) and apo-M_{2-1} (dashed line) were carried out on a Superdex 200 column equilibrated in 20 mM sodium phosphate (pH 7.0) and 0.3 M NaCl. Samples of M_{2-1} at 40 μM were incubated for 20 h at 20 °C in running buffer with or without 1 mM EDTA and 1 mM DTT. The positions of void volume (Vo), molecular size standards in kDa, and total volume (Vo + Vi) are indicated above the graph. Inset: M_{2-1} (above) and apo-M_{2-1} (below) particle size distribution determined by dynamic light scattering (DLS). Samples of M_{2-1} at 40 μM were incubated for 20 h at 20 °C prior to measurement in 20 mM sodium phosphate at pH 7.0, 1.0 M Gdm·Cl, and 1 mM DTT, with or without 1 mM EDTA.

to measure zinc reuptake, we used the PAR reagent, which reacts with free zinc and yields a strong absorbance signal at 500 nm. Apo-M_{2-1} at 4 μM was incubated with PAR and, as zinc was added, it was taken by the protein until it saturates, a point at which the zinc-PAR signal started increasing (Figure 4B). In agreement with the fluorescence CSM, the stoichiometry slightly deviated from unity.

Uncoupled Dissociation and Unfolding in Apo-M_{2-1}. We had previously shown that the unfolding and dissociation of

dx.doi.org/10.1021/bi401029q | Biochemistry 2013, 52, 6779−6789

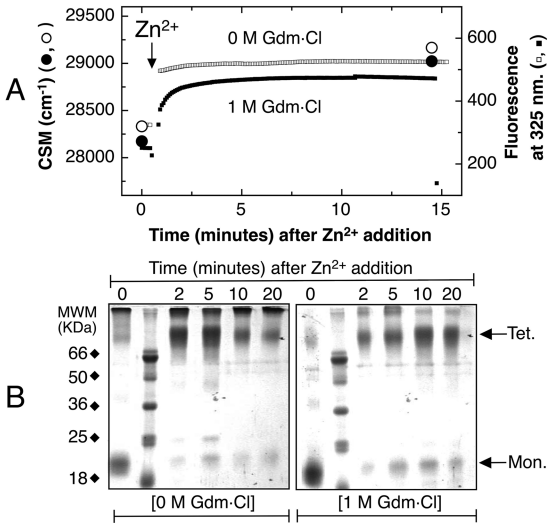

Figure 3. Monomeric apo-M_{2-1} zinc uptake promotes tetramer assembly. (A) The apo-M_{2-1} preparation was described in Experimental Procedures. Changes in the tryptophan fluorescence CSM (left Y axis) and in the fluorescence intensity at 325 nm (right Y axis) were monitored over time upon the addition of 4 μM $ZnCl_2$ to apo-M_{2-1} (2 μM) in 20 mM sodium phosphate (pH 7.0), 0.3 M NaCl, and 1 mM DTT, containing either 0 M Gdm·Cl (○, CSM; □, fluorescence intensity at 325 nm) or 1.0 M Gdm·Cl (●, CSM; ■, fluorescence intensity at 325 nm). The measurements were performed at 20 °C. (B) The samples in the same conditions as those described in A, were subjected at different time points (indicated above the graph) to glutaraldehyde cross-linking and SDS–PAGE. Left gel: the samples contained 0 M Gdm·Cl. Right gel: the samples contained 1.0 M Gdm·Cl. The molecular weights of the MWM and the bands corresponding to the tetramer and monomer are indicated.

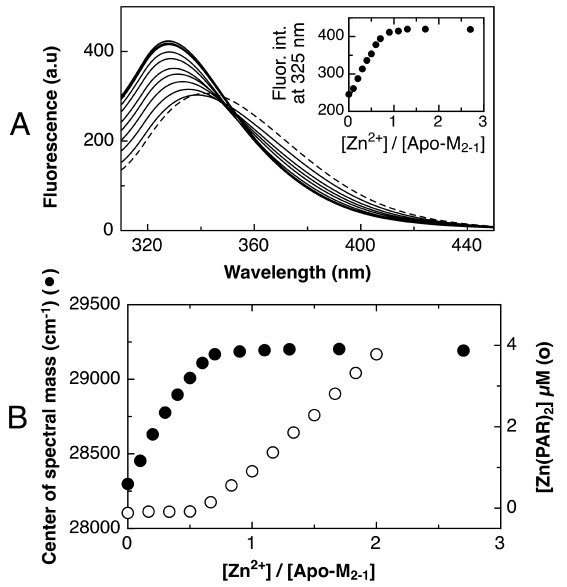

Figure 4. Apo-M_{2-1} Zn^{2+} uptake titration: (A) Apo-M_{2-1} (2 μM) was titrated with increasing amounts of $ZnCl_2$ (ranging from 0 up to 5.4 μM), and tryptophan fluorescence spectra were taken from each titration point. The dashed line represents the fluorescence spectrum of apo-M_{2-1} (0 μM Zn^{2+}). Inset: Fluorescence intensity changes at 325 nm as a function of $[Zn^{2+}]/[\text{apo-}M_{2-1}]$. (B) Left axis: Tryptophan fluorescence CSM (●) changes as a function of $[Zn^{2+}]/[\text{apo-}M_{2-1}]$. The CSM were calculated from the spectra shown in A. Right axis: titration of 100 μM PAR and 4 μM apo-M_{2-1} with increasing concentrations of $ZnCl_2$. The formation of the $Zn(PAR)_2$ complex (○) was monitored at 500 nm and plotted as a function of the $[Zn^{2+}]/[\text{apo-}M_{2-1}]$ ratio). Each titration point was incubated for 5 min, and the experiment was performed at 20 °C.

the M_{2-1} tetramer at pH 7.0 were coupled and that both fluorescence and CD signals took place in parallel through a cooperative transition[12] (Figure 5A, inset). Interestingly, while the apo-M_{2-1} secondary structure showed a stable and highly cooperative unfolding, the fluorescence CSM indicated that the tryptophan was already exposed at very low denaturant concentrations, even at 0 M Gdm·Cl (Figure 5A). However, the secondary structure transition of the apo-M_{2-1} at pH 7.0 was indistinguishable from that of the M_{2-1} tetramer (Figure 5A and inset), strongly supporting the presence of an intact and stable fold in the apo-monomer.

Glutaraldehyde cross-linking experiments coupled to SDS–PAGE analysis were carried out for determining the dissociation state along the transition. For the M_{2-1} tetramer, 2.4 M Gdm·Cl was required for complete dissociation (Figure 5 B, left panel), which nevertheless required full unfolding of the tetramer (Figure 5A, inset, and ref 12). In the case of the apo-monomer, the tetramer was fully dissociated already between 0 and 0.2 M denaturant, indicating that the equilibrium was strongly shifted to the monomer in the apo-species (Figure 5B, right panel). Analysis of the transition showed a clear two-state behavior from folded to unfolded monomer. The process is described by a free energy change of unfolding (ΔG^{UNF}) of 6.22 ± 0.36 kcal/mol and an m cooperativity value of 2.8 ± 0.16 kcal/mol·M, where the fitting curve for the ellipticity transition data is shown in Figure 5A.

We had previously shown that the dissociation-unfolding of the M_{2-1} tetramer was strongly influenced by pH, with a K_D of 10^{-28} M^3 at pH 7.0 and 10^{-18} M^3 at pH 5.0.[12] Even though we could infer that the M_{2-1} tetramer was less stable at pH 5.0, we did not have direct data obtained from denaturation experiments at that time. Here, we show that at pH 5.0 the denaturation transition was clearly uncoupled, where the fluorescence change largely precedes that of the secondary structure change (Figure 6A). This indicates that, as expected, the association of the holo-tetramer is weaker at pH 5.0 and is uncoupled from global folding. The unfolding of the apo-M_{2-1} was also uncoupled; at zero denaturant, the species was already monomeric, confirmed by SEC and DLS experiments, whereas the M_{2-1} oligomeric state at pH 5.0 was tetrameric (Figure 6B and inset). The hydrodynamic behavior of M_{2-1} and apo-M_{2-1}, determined in a Superdex 200 column, corresponded to 115 and 32 kDa globular species, respectively. Consistent with this, the hydrodynamic diameter determined by DLS was 8.72 ± 1.75 nm for M_{2-1} and 6.43 ± 1.25 nm for apo-M_{2-1}, corresponding to 131 kDa and 57 kDa globular species.[33] At pH 5.0, both the M_{2-1} tetramer and apo-M_{2-1} monomer showed a cooperative two-state transition of its secondary structure corresponding to global unfolding. The monomer was also less stable at pH 5.0 (ΔG^{UNF} = 4.01 ± 0.54 kcal/mol) compared to that at pH 7.0 (ΔG^{UNF} = 6.22 ± 0.36 kcal/mol) described above, with an m value at pH 5.0 of 2.15 ± 0.2 kcal/mol·M compared to 2.8 at pH 7.0. The m value for the transition at pH 7.0 corresponded to changes in accessible surface area (ΔASA) of 8822 Å^2 while at pH 5.0 corresponded to a ΔASA of 5868 Å^2.[34]

Interplay between Redox and pH on the Tetramer-Apo-Monomer Equilibrium. This particular zinc-binding motif, as in other similar but not identical ones, consists of a

dx.doi.org/10.1021/bi401029q | Biochemistry 2013, 52, 6779–6789

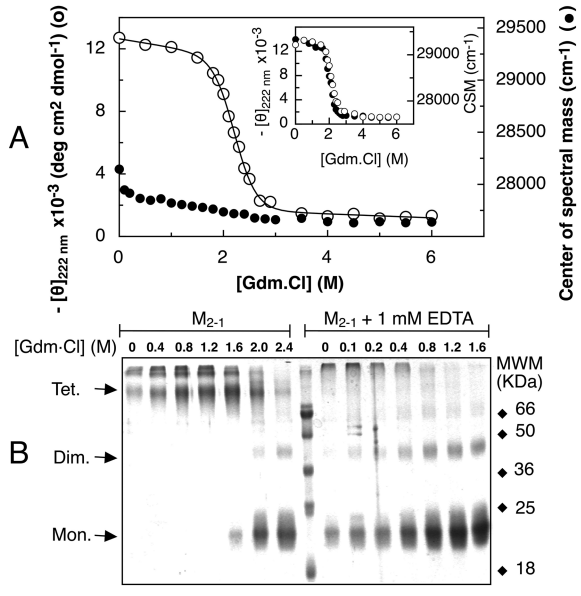

Figure 5. Gdm·Cl equilibrium unfolding of apo-M_{2-1} at pH 7.0. (A) Apo-M_{2-1} equilibrium unfolding transition followed by monitoring molar ellipticity at 222 nm (○) and tryptophan fluorescence center of spectral mass (●). The CD data were fit to a two-state unfolding model using the eq 3 and is plotted as a solid line. M_{2-1} (5 μM) was incubated for 16 h at 20 °C in 20 mM sodium phosphate (pH 7.0), 0.3 M NaCl, 1 mM DTT, 1 mM EDTA, and increasing Gdm·Cl concentrations. Inset: GdmCl equilibrium unfolding of M_{2-1} at pH 7.0 monitored by the changes in molar ellipticity at 222 nm (○) and fluorescence CSM (●). The incubation conditions were the same described above but without adding 1 mM EDTA to the samples. (B) Quaternary structure of apo-M_{2-1} as a function of Gdm·Cl concentration. After the spectroscopic measurements shown in A, the samples were subjected to glutaraldehyde cross-linking, SDS–PAGE, and Coomasie-blue staining. On the left side of the molecular weight marker (MWM) is shown M_{2-1} with increasing Gdm·Cl concentrations (indicated above the graph). At the right side of the MWM is shown apo-M_{2-1} with increasing Gdm·Cl concentrations. The tetramer, monomer, and dimer bands are indicated on the left side, and the molecular weights of the MWM are indicated on the right side of the gel.

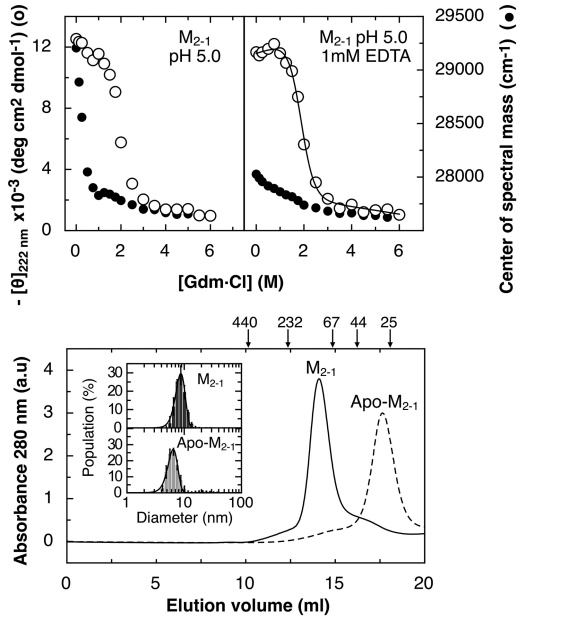

Figure 6. Gdm·Cl equilibrium unfolding of M_{2-1} and apo-M_{2-1} at pH 5.0 (A). M_{2-1} (left graph) and apo-M_{2-1} (right graph) equilibrium unfolding transition followed by monitoring changes in molar ellipticity at 222 nm (○) and tryptophan fluorescence CSM (●). The M_{2-1} protein at 5 μM was incubated at 20 °C for 16 h in 20 mM sodium acetate (pH 5.0), 0.2 M NaCl, 1 mM DTT, and increasing Gdm·Cl concentrations. Apo-M_{2-1} was prepared in each incubation tube by adding 1 mM EDTA. The two-state model fitting of apo-M_{2-1} denaturation is plotted as a solid line. (B) Size exclusion chromatographies of M_{2-1} (solid line) and apo-M_{2-1} (dashed line) were carried out on a Superdex 200 column equilibrated in 20 mM sodium acetate (pH 5.0) and 0.2 M NaCl. Samples of M_{2-1} (40 μM) were incubated at 20 °C for 2–3 h in 20 mM sodium acetate (pH 5.0), 0.2 M NaCl, and 1 mM DTT, with or without 1 mM EDTA. After the incubation period, the samples were subjected first to DLS measurements (inset) and then run on a S200 SEC. The positions of void volume (Vo), molecular size standards in kDa, and total volume (Vo + Vi) are indicated above the graph. Inset: M_{2-1} (above) and apo-M_{2-1} (below) particle size distribution determined by DLS.

combination of cysteine and histidine residues. As a consequence, the strength by which the metal binds to the site and therefore the modulation of the oligomerization equilibria in RSV M_{2-1} could be influenced by pH as well as the redox state. We next sought to characterize the redox effect and quantify the extent of influence of both parameters. A simple and straightforward first approach to perturb the redox state is to oxidize the M_{2-1} tetramer by adding hydrogen peroxide. Introducing this oxidizing reagent into the protein solution caused a release of over 80% of the zinc content, which was accelerated at 37 °C compared to 20 °C (Figure 7A). The release of zinc induced by H_20_2 treatment led to dissociation to monomer as determined by SEC experiments (not shown).

As a more accurate approach, we wanted to evaluate the effect of the redox state in a wide range of conditions by using a mixture of oxidized (GSSG) and reduced (GSH) glutathione redox buffers. Ratios of GSH/GSSG between 1 to 10 are associated with oxidative stress, whereas ratios between 10 to 300 are associated with physiological redox potentials. Since we showed that changes in tryptophan fluorescence CSM were a highly sensitive probe for dissociation after zinc removal, we monitored this signal at either pH 7.0 or 5.0 with different GSH/GSSG ratios, compatible with oxidative stress and physiological conditions. Throughout the GSH/GSSG ranges tested at pH 7.0, we found no change in the CSM, suggesting that the oxidative stress conditions created by the GSH/GSSG ratios below 10 could not alone oxidize the coordinating cysteines, thus promoting zinc release and M_{2-1} tetramer dissociation. Conversely, at pH 5.0, the tryptophan was already exposed to the solvent along all the GSH/GSSG ratios tested, indicating that at this pH the monomeric apo-M_{2-1} was formed. We have shown above that M_{2-1} at pH 5.0 in sodium acetate buffer was tetrameric (Figure 6B), which is not in agreement with the results obtained using glutathione buffer at pH 5.0. To clarify this, we evaluated the pH dependence of M_{2-1} dissociation using buffers with and without glutathione. In the absence of GSH/GSSG, the tetrameric to monomeric transition midpoint was at pH 4.7 and the monomeric form, which we assume to be apo-M_{2-1}, was highly populated at pH 4.5 (Figure 7C). However, the addition of GSH/GSSG, at ratios from 1 to 300, produced an earlier pH dissociation onset (Figure 7C). The midpoint transition was shifted to pH 5.2, and the monomeric form was highly populated at pH 5.0. The first conclusion from this experiment is that there is not a direct effect of the redox state of the chemical environment, which

dx.doi.org/10.1021/bi401029q | Biochemistry 2013, 52, 6779–6789

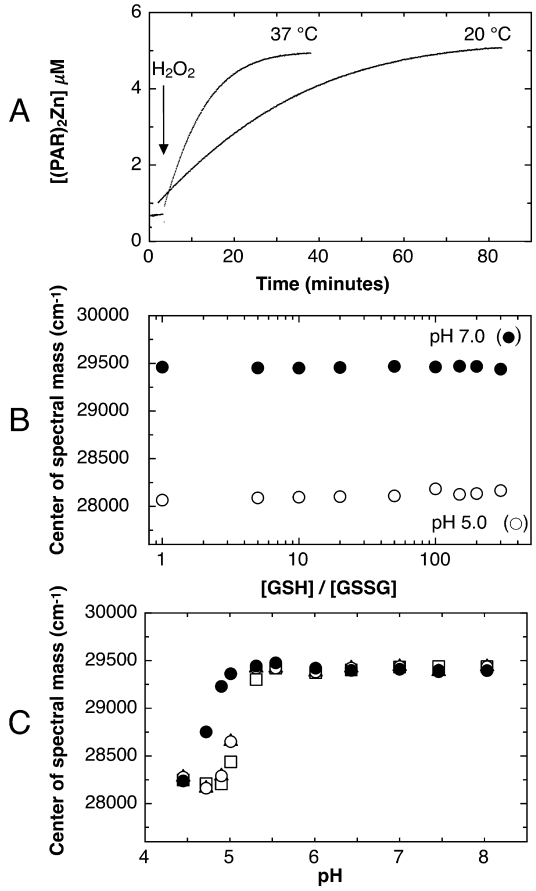

Figure 7. M_{2-1} CCCH motif redox-state and pH dependence. (A) Oxidation of M_{2-1} by hydrogen peroxide. M_{2-1} without DTT at 6 μM was incubated with H_2O_2 (3 mM) in sodium phosphate (pH 7.0) and 0.3 M NaCl at either 20 or 37 °C. Zinc release from M_{2-1} upon oxidation was monitored over time at 500 nm, indicative of the formation of the $Zn(PAR)_2$ complex. (B) Tryptophan fluorescence CSM of M_{2-1} as a function of GSH/GSSG ratios at either pH 7.0 (●) or pH 5.0 (○). Samples of M_{2-1} at 6 μM were incubated for 16 h at 20 °C in 20 mM sodium phosphate at pH 7.0 or 20 mM sodium acetate at pH 5.0, both with 0.2 M NaCl and 5 mM final concentration of GSH/GSSG mixtures. (C) Tryptophan fluorescence CSM mass of M_{2-1} at different pH values and GSH/GSSG ratios. M_{2-1} at 6 μM was incubated for 16 h at 20 °C in broad range buffer (50 mM Tris-HCl, 25 mM MES, 25 mM sodium acetate, and 0.2 M NaCl) without glutathione (●) or with GSH/GSSG ratios of 1 (○), 100 (□), and 300 (Δ). The pH values of the solutions range from 4.4 to 8.4.

would in principle be reflected by the lack of change in the pH titration. Surprisingly, the shift in the pH titration indicates that the GSH/GSSG is acting as a chelating agent and removes the metal to yield the apo-monomer starting at pH 5.3 (Figure 7C). However, there is no such zinc release event at pH 7.0 caused by the glutathione, as the fluorescence CSM signal remains unchanged. Altogether, these observations suggested that at pH 5.0 the CCCH motif zinc affinity was lower than at pH 7.0, and glutathione chelated zinc at pH 5.0, promoting tetramer dissociation.

Binding of RNA by the Apo-M_{2-1} Monomer and Outcompetition by the RSV Phospohoprotein P. As required by its functional role, M_{2-1} binds RNA, with no specific sequence preference described so far.[16,18] As a straightforward test for this, we used tRNA as the binding ligand and carried out an EMSA assay. Gradual addition of the M_{2-1} holo-tetramer caused a shift of the free tRNA band into the protein−RNA complex (Figure 8A, top). Interestingly, the process was completed at an ∼1:1 tRNA/M_{2-1} tetramer ratio, which indicates that given the extreme tightness of the tetramer at pH 7.0, there can be 1 tRNA molecule per M_{2-1} tetramer molecule. Identical shift results were obtained with the apo-M_{2-1} monomer (Figure 8A, bottom), which indicates that the lack of zinc affected neither the stoichiometry nor the affinity for this unspecific ligand.

The RSV P is an essential cofactor of the L RNA polymerase, thus partaking in the architecture of the RNA polymerase complex.[5] It is also a tight tetramer, incidentally with affinity indistinguishable from that of the M_{2-1} tetramer.[19] They were described to interact,[11,35] and they do so with nanomolar affinity in solution[19] forming a unique tetramer−tetramer interface. In order to test whether P and RNA compete for binding to the M_{2-1} tetramer or apo-monomer, we coincubated M_{2-1} and the apo-M_{2-1} monomer with tRNA under conditions that ensured full formation of the complex (see Experimental Procedures), with increasing amounts of P. At pH 7.0, P outcompeted the RNA at exactly a 1:1 stoichiometric ratio with M_{2-1} (10 μM P/10 μM M_{2-1}) (Figure 8B, top), in excellent agreement with what we had previously described.[19] An identical result is observed for apo-M_{2-1} (Figure 8B, bottom). The direct interaction between apo-M_{2-1} and P was further confirmed by SEC experiments, followed by precipitation of the peak and analysis by SDS−PAGE (not shown).

■ DISCUSSION

A complex network of protein−protein and RNA−protein interactions, involved in RSV transcription and replication, take place between M_{2-1}, P, L, N, and RNA.[5] Moreover, an interaction between M_{2-1} and the matrix (M) protein has been associated with virus assembly and budding.[10] Thus, M_{2-1} seems to play a key role in the RSV virus life cycle. The RSV M_{2-1} protein harbors a conserved CCCH zinc-binding motif, which is essential to maintain the functional integrity of M_{2-1} and for viral viability.[13,14] However, the exact role that the CCCH motif plays in M_{2-1} protein structure and function is still unknown.

In order to tackle the analysis of the role of CCCH zinc binding in M_{2-1} structure, conformational stability, and RNA and P binding, we monitored the conformational changes induced by zinc removal. The single M_{2-1} tryptophan (W30) was an ideal fluorescence spectroscopic probe to monitor tetramer dissociation. It is located between the CCCH motif (residues 7 to 25) and the oligomerization domain (residues 32 to 63).[11] In the tetrameric state, the tryptophan is buried from the solvent, while the dissociation caused by zinc release exposes the tryptophan to the solvent. Chemical cross-linking, DLS, and SEC experiments validate the use of tryptophan fluorescence as a high sensitive probe for monitoring the M_{2-1} dissociation equilibrium. Our results indicate that the dissociation mediated by zinc release leaves the secondary structure intact and stable, as judged by far UV-CD and unfolding experiments. Furthermore, a preparation of the apo-M_{2-1} monomer readily reuptakes zinc and returns to the native M_{2-1} tetramer. However, Tran et al.[11] reported that an N-terminal deletion mutant of 31 residues lacking the CCCH motif ($M_{2-1}\Delta$31N) retained the ability to oligomerize, while we now show that that zinc binding to the CCCH motif is essential for the tetramer assembly. This difference could be due to the fact that they analyzed the tetramerization by performing

dx.doi.org/10.1021/bi401029q | Biochemistry 2013, 52, 6779−6789

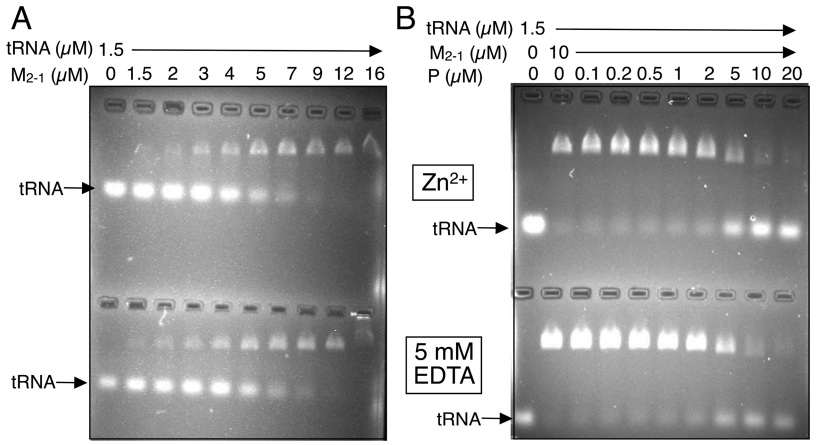

Figure 8. Electrophoretic mobility shift assay (EMSA) of M_{2-1}:tRNA and apo-M_{2-1}:tRNA complexes and competition experiments with P. (A) Increasing concentrations of purified M_{2-1} were incubated with 1.5 μM tRNA and subjected to Tris-acetate 1.5% agarose gel electrophoresis, stained with ethidium bromide and visualized under UV light. The upper lanes of the gel show the M_{2-1}:tRNA complexes with 10 μM zinc, and the lower lanes show the apo-M_{2-1}:tRNA complexes, in the presence of 5 mM EDTA. The binding process was completed at an ~1:1 tRNA/M_{2-1} tetramer ratio (1.5 μM of tRNA/9 μM of M_{2-1} monomer or 2.25 μM of M_{2-1} tetramer). (B) Increasing concentrations of purified P were incubated with 1.5 μM tRNA and 10 μM M_{2-1} and then subjected to Tris-acetate 1.5% agarose gel electrophoresis. The upper lanes of the gel show the P:M_{2-1}:tRNA complexes with 10 μM zinc, and the lower lanes show the P:apo-M_{2-1}:tRNA complexes incubated with 5 mM EDTA. All of the samples were incubated at 4 °C for 6 h prior to electrophoresis.

copurification of the GST-M_{2-1}Δ31N protein with the histidine-tag-fused wild type M_{2-1} (*wt* His-M_{2-1}). The *wt* His-M_{2-1} protein harbors an intact CCCH motif, and we speculate that at least two atoms of zinc must be present to allow the heterotetrameric interaction of $(\text{His-M}_{2-1})_2/(\text{GST-M}_{2-1}\Delta 31\text{N})_2$. A homotetrameric assembly of GST-M_{2-1}Δ31N should therefore not be viable. Consistent with our results, the secondary structure content of this deletion mutant was similar to that of full length apo-M_{2-1}, suggesting that this motif does not contribute to the full length M_{2-1} α-helical content, which is determined mainly by the folded domain with α-helical structure spanning from residues 74 to 151, in agreement with the NMR data.[18]

As was previously shown for the tetrameric M_{2-1},[11] the apo-M_{2-1} protein was able to interact with tRNA and P in a competitive manner. These findings indicate that the apo-M_{2-1} monomer is able to interact either with P and unspecific RNA and that M_{2-1} homo-oligomerization is not essential for both interactions. A deletion mutant (M_{2-1} Δ58N) with both the CCCH motif and the oligomerization domain removed retained the ability to bind RNA and P[11] in agreement with the monomeric apo-M_{2-1} protein described here. Interestingly, a deletion mutant lacking residues 35 to 58 was not able to oligomerize and lost its transcription antiterminator activity in functional assays,[11] suggesting that the monomeric apo-M_{2-1} could also be inactive, the equivalent of the antitermination incompetent natural species possibly being modulated by zinc removal within the viral replication cycle in the host cell.

Moreover, individual mutation of the three residues that coordinate zinc (Cys7, Cys15, and His25) prevented the M_{2-1} protein from enhancing transcriptional read-through and interacting with the nucleocapsid protein,[13] and also impaired viral viability.[14] An important conclusion is that what was defined as an oligomerization domain by deletion is not strictly the case since the protein dissociates readily by removal of the zinc from the full-length species, where the sequence information of this putative domain is present. However, a mutant lacking the oligomerization domain (residues 35−58) was unable to homo-oligomerize.[11] Consequently, although the M_{2-1} oligomerization domain is required for tetramerization, the latter is strongly modulated by zinc binding and removal from the Cys_3His_1 motif. In other words, the oligomerization domain does not have the capacity to form a tight tetramer in the absence of the Cys_3His_1 motif, and this motif should be included as part of the tetramerization domain. This could to be addressed by determining whether a 23 amino acid peptide comprising the oligomerization domain forms a tetramer, constituting an independent domain.

With respect to the folding stability, the apo-monomer is 2.2 kcal mol^{-1} more stable at pH 7.0 than at pH 5.0. On the basis of the established correlation between *m* values (the slope of the unfolding transition) and the change in exposure of the surface area (ΔASA) to the solvent,[34] an increase in *m* value of 0.6 kcal mol^{-1} M^{-1} at pH 7.0 indicates at least a 40% increase in buried ASA (see Results). Since it is safe to assume that the unfolded states at the two pH values will be similar in terms of ASA, we can conclude that the apo-M_{2-1} monomer at pH 5.0 has more solvent accessible regions. However, the small change in CD with respect to pH 7.0 and the strong unfolding cooperativity suggest that a subdomain other than the main two-state unfolding core domain could exist. Alternatively, the increased ASA at pH 5.0 could be at least in part due to increased solvent accessibility to internal sites. On the basis of an extremely tight correlation between ΔASA and the number of residues in fully folded globular proteins with known structure,[34] the *m* value and therefore the ΔASA of apo-M_{2-1} correspond to that of a globular domain of ~100 residues in good agreement with the independently folded core domain of 120 residues whose structure was determined by NMR.[18] Moreover, 16 of the 120 residues were reported to be disordered.

We had previously shown that a partly folded monomeric intermediate was populated in the dissociation-unfolding transition of tetrameric holo M_{2-1} at pH 7.0, with a ΔG of 5.6 kcal mol^{-1}.[12] This intermediate species was defined as a late molten globule, where secondary and tertiary structures are not fully compacted. This species differs substantially from the native-like apo-monomer formed after the removal of zinc,

dx.doi.org/10.1021/bi401029q | *Biochemistry* 2013, 52, 6779−6789

revealing that the coupled dissociation-unfolding is completely absent in this species.

Many redox-regulated proteins have highly reactive cysteines that undergo reversible thiol modifications in response to reactive oxygen or nitrogen oxide species, which, in turn, leads to changes in protein structure, function, activity, or localization. The fact that *in vitro* oxidation by H_2O_2 promotes M_{2-1} zinc release and tetramer dissociation allowed us to hypothesize that the M_{2-1} CCCH motif could be acting as a redox switch. However, the range for cysteine oxidation determined was rather extreme and unlikely to be functional. Using the GSH/GSSG redox couple, we found that GSH or GSSG modified the redox balance by acting as chelating agents and promote dissociation. The zinc-chelating activity of glutathione species was previously reported,[36] and the high *in vivo* concentrations of GSH/GSSG cannot rule out its participation *in vivo*. The chelating activity took place at pH 5.0 only, suggesting a combined role with histidine protonation, in agreement with the strong pH dependence of the dissociation we showed for the M_{2-1} tetramer.

There are many examples of zinc-binding motifs bridging the interaction interface between proteins. The mammalian voltage-gated potassium channels of the Kv family assemble into homomeric or heteromeric tetramers to form functional channels. The Shaw (Kv3) tetramerization domain structure reveals one zinc per monomer tetrahedrally coordinated at the assembly interface by a C_3H_1 motif ($HX_5CX_{20}CC$), with one histidine and two cysteine residues contributed by one monomer and one cysteine from an adjacent monomer.[37] These four amino acids are located in the subunit interface, and in this case, the zinc ion promotes intersubunit contacts. Another case is Human MCM10 (minichromosomal maintenance protein 10) that acts as a DNA replication factor that self-interacts and assembles into homohexameric complexes.[38] In the yeast Mcm10 protein, it was shown that a $CX_{10}CX_{11}CX_2H$ motif is essential for the homocomplex formation and that substitutions in the coordinating residues abolished homocomplex assembly. Interestingly, EDTA incubation also disrupted yeast Mcm10 self-interaction.[39] A third example of zinc-induced tetramerization is represented by the HIV-1 Integrase. In this case, zinc binding to the HHCC motif stabilizes the N-terminal domain and promotes tetramerization.[40] Similar to the case of the RSV M_{2-1} protein, the *in vitro* recombinant HIV-1 Integrase apoprotein yields mainly monomeric species, while metal binding induced multimerization.[41] Experimental evidence showed that HIV-1 Integrase forms stable homotetramers *in vivo*.[42] Altogether, these different examples converge in a role of dissociation and modulation of protein function by zinc Cys-His motifs.

Overall, M_{2-1} dissociation induced by zinc release, by a pH switch, metal chelation, or more likely, a combination of both, together with a redox component, could represent a main regulatory mechanism affecting M_{2-1} protein function in its different expressions (antitermination, replication, virus assembly, and budding) and context. Given the ability of M_{2-1} to interact with different RSV proteins and RNA and the fact that many of these proteins can generate multicomplexes of different components, a sensitive and fast modulation of an otherwise extremely tight tetramerization process is likely to be a highly relevant event in the RSV life cycle. The most obvious situation will be the formation of the RNA polymerase complex and how its composition may be modified for transcription or replication scenarios.

AUTHOR INFORMATION

Corresponding Author

*Phone: + 54 11 5238 7500, ext. 3209. Fax: + 54 11 5238 7501. E-mail: gpg@leloir.org.ar

Funding

This work was supported by grants CRP/ARG10-02 from the International Centre for Biotechnology (ICGEB), PIP 11220110100288 from CONICET, and PICT-2011-0721 from ANPCyT. M.G.N. holds a graduate fellowship from Consejo Nacional de Investigaciones Científicas y Técnicas (CONICET); S.A.E. and G.D.P.G. are CONICET Career Investigators.

Notes

The authors declare no competing financial interest.

ACKNOWLEDGMENTS

We thank Lucia B. Chemes for helpful assistance and discussions regarding unfolding experiments.

ABBREVIATIONS

RSV, respiratory syncytial virus; Gdm·Cl, guanidinium chloride; CD, circular dichroism; CSM, center of spectral mass; SEC, size exclusion chromatography; DLS, dynamic light scattering; DTT, dithiothreitol; PAR, 4-(2-pyridylazo)-resorcinol; PMPS, *p*-hydroxymercuri-phenylsulfonic acid; EDTA, ethylenediaminetetraacetic acid; GSH/GSSG, glutathione/glutathione disulfide redox couple

REFERENCES

(1) Schickli, J. H., Dubovsky, F., and Tang, R. S. (2009) Challenges in developing a pediatric RSV vaccine. *Hum. Vaccines 5*, 582−591.

(2) Murata, Y., and Falsey, A. R. (2007) Respiratory syncytial virus infection in adults. *Antiviral Ther. 12*, 659−670.

(3) Meissner, H. C., Rennels, M. B., Pickering, L. K., and Hall, C. B. (2004) Risk of severe respiratory syncytial virus disease, identification of high risk infants and recommendations for prophylaxis with palivizumab. *Pediatr. Infect. Dis. J. 23*, 284−285.

(4) Ventre, K., and Randolph, A. G. (2007) Ribavirin for respiratory syncytial virus infection of the lower respiratory tract in infants and young children. *Cochrane Database Syst. Rev.*, CD000181.

(5) Collins, P. L., Chanock, R. M., Murphy, B. R. (2001) Respiratory Syncytial Virus. in *Fields Virology,* (Fields, B. N., Knipe, D. M., Griffin, D. E., Lamb, R. A., Martin, M. A., Roizman, B, and Straus, S. E., Eds.) 4th ed., Lippincott Williams & Wilkins Publishers, Philadelphia, PA.

(6) Collins, P. L., Hill, M. G., Cristina, J., and Grosfeld, H. (1996) Transcription elongation factor of respiratory syncytial virus, a nonsegmented negative-strand RNA virus. *Proc. Natl. Acad. Sci. U.S.A. 93*, 81−85.

(7) Fearns, R., and Collins, P. L. (1999) Role of the M2−1 transcription antitermination protein of respiratory syncytial virus in sequential transcription. *J. Virol. 73*, 5852−5864.

(8) Hardy, R. W., Harmon, S. B., and Wertz, G. W. (1999) Diverse gene junctions of respiratory syncytial virus modulate the efficiency of transcription termination and respond differently to M2-mediated antitermination. *J. Virol. 73*, 170−176.

(9) Garcia, J., Garcia-Barreno, B., Vivo, A., and Melero, J. A. (1993) Cytoplasmic inclusions of respiratory syncytial virus-infected cells: formation of inclusion bodies in transfected cells that coexpress the nucleoprotein, the phosphoprotein, and the 22K protein. *Virology 195*, 243−247.

(10) Li, D., Jans, D. A., Bardin, P. G., Meanger, J., Mills, J., and Ghildyal, R. (2008) Association of respiratory syncytial virus M protein with viral nucleocapsids is mediated by the M2−1 protein. *J. Virol. 82*, 8863−8870.

(11) Tran, T. L., Castagne, N., Dubosclard, V., Noinville, S., Koch, E., Moudjou, M., Henry, C., Bernard, J., Yeo, R. P., and Eleouet, J. F. (2009) The respiratory syncytial virus M2−1 protein forms tetramers and interacts with RNA and P in a competitive manner. *J. Virol. 83*, 6363−6374.
(12) Esperante, S. A., Chemes, L. B., Sanchez, I. E., and de Prat-Gay, G. (2011) The respiratory syncytial virus transcription antiterminator M(2−1) is a highly stable, zinc binding tetramer with strong pH-dependent dissociation and a monomeric unfolding intermediate. *Biochemistry 50*, 8529−8539.
(13) Hardy, R. W., and Wertz, G. W. (2000) The Cys(3)-His(1) motif of the respiratory syncytial virus M2−1 protein is essential for protein function. *J. Virol. 74*, 5880−5885.
(14) Tang, R. S., Nguyen, N., Cheng, X., and Jin, H. (2001) Requirement of cysteines and length of the human respiratory syncytial virus M2−1 protein for protein function and virus viability. *J. Virol. 75*, 11328−11335.
(15) Zhou, H., Cheng, X., and Jin, H. (2003) Identification of amino acids that are critical to the processivity function of respiratory syncytial virus M2−1 protein. *J. Virol. 77*, 5046−5053.
(16) Cuesta, I., Geng, X., Asenjo, A., and Villanueva, N. (2000) Structural phosphoprotein M2−1 of the human respiratory syncytial virus is an RNA binding protein. *J. Virol. 74*, 9858−9867.
(17) Hartlieb, B., Muziol, T., Weissenhorn, W., and Becker, S. (2007) Crystal structure of the C-terminal domain of Ebola virus VP30 reveals a role in transcription and nucleocapsid association. *Proc. Natl. Acad. Sci. U.S.A. 104*, 624−629.
(18) Blondot, M. L., Dubosclard, V., Fix, J., Lassoued, S., Aumont-Nicaise, M., Bontems, F., Eleouet, J. F., and Sizun, C. (2012) Structure and functional analysis of the RNA- and viral phosphoprotein-binding domain of respiratory syncytial virus M2−1 protein. *PLoS Pathog. 8*, e1002734.
(19) Esperante, S. A., Paris, G., and de Prat-Gay, G. (2012) Modular unfolding and dissociation of the human respiratory syncytial virus phosphoprotein p and its interaction with the m(2−1) antiterminator: a singular tetramer-tetramer interface arrangement. *Biochemistry 51*, 8100−8110.
(20) Hall, T. M. (2005) Multiple modes of RNA recognition by zinc finger proteins. *Curr. Opin. Struct. Biol. 15*, 367−373.
(21) Brown, R. S. (2005) Zinc finger proteins: getting a grip on RNA. *Curr. Opin. Struct. Biol. 15*, 94−98.
(22) Sun, L., Liu, A., and Georgopoulos, K. (1996) Zinc finger-mediated protein interactions modulate Ikaros activity, a molecular control of lymphocyte development. *EMBO J. 15*, 5358−5369.
(23) Brooks, S. A., and Blackshear, P. J. (2013) Tristetraprolin (TTP): Interactions with mRNA and proteins, and current thoughts on mechanisms of action. *Biochim. Biophys. Acta 1829*, 666−679.
(24) Michel, S. L., Guerrerio, A. L., and Berg, J. M. (2003) Selective RNA binding by a single CCCH zinc-binding domain from Nup475 (Tristetraprolin). *Biochemistry 42*, 4626−4630.
(25) Amann, B. T., Worthington, M. T., and Berg, J. M. (2003) A Cys3His zinc-binding domain from Nup475/tristetraprolin: a novel fold with a disklike structure. *Biochemistry 42*, 217−221.
(26) Hudson, B. P., Martinez-Yamout, M. A., Dyson, H. J., and Wright, P. E. (2004) Recognition of the mRNA AU-rich element by the zinc finger domain of TIS11d. *Nat. Struct. Mol. Biol. 11*, 257−264.
(27) Lu, P., Lu, G., Yan, C., Wang, L., Li, W., and Yin, P. (2012) Structure of the mRNA splicing complex component Cwc2: insights into RNA recognition. *Biochem. J. 441*, 591−597.
(28) John, S. P., Wang, T., Steffen, S., Longhi, S., Schmaljohn, C. S., and Jonsson, C. B. (2007) Ebola virus VP30 is an RNA binding protein. *J. Virol. 81*, 8967−8976.
(29) Modrof, J., Becker, S., and Muhlberger, E. (2003) Ebola virus transcription activator VP30 is a zinc-binding protein. *J. Virol. 77*, 3334−3338.
(30) Hartlieb, B., Modrof, J., Muhlberger, E., Klenk, H. D., and Becker, S. (2003) Oligomerization of Ebola virus VP30 is essential for viral transcription and can be inhibited by a synthetic peptide. *J. Biol. Chem. 278*, 41830−41836.
(31) Hunt, J. B., Neece, S. H., and Ginsburg, A. (1985) The use of 4-(2-pyridylazo)resorcinol in studies of zinc release from Escherichia coli aspartate transcarbamoylase. *Anal. Biochem. 146*, 150−157.
(32) Pace, C. N. (1986) Determination and analysis of urea and guanidine hydrochloride denaturation curves. *Methods Enzymol. 131*, 266−280.
(33) Uversky, V. N. (2002) Natively unfolded proteins: a point where biology waits for physics. *Protein Sci. 11*, 739−756.
(34) Myers, J. K., Pace, C. N., and Scholtz, J. M. (1995) Denaturant m values and heat capacity changes: relation to changes in accessible surface areas of protein unfolding. *Protein Sci. 4*, 2138−2148.
(35) Mason, S. W., Aberg, E., Lawetz, C., DeLong, R., Whitehead, P., and Liuzzi, M. (2003) Interaction between human respiratory syncytial virus (RSV) M2-1 and P proteins is required for reconstitution of M2-1-dependent RSV minigenome activity. *J. Virol. 77*, 10670−10676.
(36) Krezel, A., and Bal, W. (2004) Studies of zinc(II) and nickel(II) complexes of GSH, GSSG and their analogs shed more light on their biological relevance. *Bioinorg. Chem. Appl.*, 293−305.
(37) Bixby, K. A., Nanao, M. H., Shen, N. V., Kreusch, A., Bellamy, H., Pfaffinger, P. J., and Choe, S. (1999) Zn2+-binding and molecular determinants of tetramerization in voltage-gated K+ channels. *Nat. Struct. Biol. 6*, 38−43.
(38) Okorokov, A. L., Waugh, A., Hodgkinson, J., Murthy, A., Hong, H. K., Leo, E., Sherman, M. B., Stoeber, K., Orlova, E. V., and Williams, G. H. (2007) Hexameric ring structure of human MCM10 DNA replication factor. *EMBO Rep. 8*, 925−930.
(39) Cook, C. R., Kung, G., Peterson, F. C., Volkman, B. F., and Lei, M. (2003) A novel zinc finger is required for Mcm10 homocomplex assembly. *J. Biol. Chem. 278*, 36051−36058.
(40) Zheng, R., Jenkins, T. M., and Craigie, R. (1996) Zinc folds the N-terminal domain of HIV-1 integrase, promotes multimerization, and enhances catalytic activity. *Proc. Natl. Acad. Sci. U.S.A. 93*, 13659−13664.
(41) Lee, S. P., Xiao, J., Knutson, J. R., Lewis, M. S., and Han, M. K. (1997) Zn2+ promotes the self-association of human immunodeficiency virus type-1 integrase in vitro. *Biochemistry 36*, 173−180.
(42) Cherepanov, P., Maertens, G., Proost, P., Devreese, B., Van Beeumen, J., Engelborghs, Y., De Clercq, E., and Debyser, Z. (2003) HIV-1 integrase forms stable tetramers and associates with LEDGF/p75 protein in human cells. *J. Biol. Chem. 278*, 372−381.